Arch. Metall. Mater. **69** (2024), 2, 775-782

DOI: https://doi.org/10.24425/amm.2024.149809

B. KUMAR[1*], A.K. SAHU[2], D. DAS[3], S. BAG[3]

PROBING THE THERMAL STABILITY AND MICROSTRUCTURAL-MECHANICAL BEHAVIOUR OF LASER-WELDED 17-4 PH STAINLESS STEEL

Dissimilar-weld-fabrications are created to capture privilege of certain attributes of each component to enhance the potential of overall structure. Induced residual stress owing to non-uniform thermal cycle, strain developed by virtue of metallurgical-transformation, and dramatic difference in thermo-physical and thermo-mechanical property, proved to be a major drawback and limits application certainly. Present study includes amalgamation of material-characterization and numerical-modelling to overcome aforementioned issue. The 17-4 precipitation-hardened steel was joined with SS316 steel by CO_2 laser-welding technique using different-heat-input. It is noticed that the distribution and amount of δ-ferrite controls the on-site behavior relating to thermal stability, microstructural characteristics and residual stress generation. This work is attempted to understand thermal behavior as well as its correlation with δ-ferrite formation and residual stress distribution. Sequential-coupled-thermo-mechanical model proposed to developed for dissimilar weld joints at different process conditions. Finally, the interrelation between microstructure and the typical pattern of residual stress believed to be investigated systematically.

Keywords: Dissmilar welding; finite element model; thermo-microstructure-mechanical characterization; thermal behaviour estimation

1. Introduction

Laser Beam Welding (LBW) is a high-density power, rapid, and non-contact type joining process. The high-power density of LBW process allows for achieving good depth of penetration, whereas narrow welds allow to reduce the size of heat affected zone (HAZ) in the welded products. The LBW find applications in various power plant, petrochemical, and nuclear industries due to high productivity, good repeatability, and high efficiency [1]. Hence, LBW technique is currently used for welding various steel grades in similar and dissimilar configurations [2,3]. Although, LBW is a relatively old joining technique, and the application of stainless steel (SS) is well established in various industries. However, the literature lacks a comprehensive investigation of the dissimilar welding of 17-4 PH SS to austenitic stainless steel (ASS) 304.

The 17-4 PH is a martensitic SS and exhibits high strength and good toughness along with good corrosion resistance and is widely used in the aerospace industry, missile fittings, jet engine parts, and nuclear reactor components [4]. The ASS 304 is used in nuclear power plants, chemical reactors, pulp and paper industry due to its low cost, good mechanical properties, and corrosion resistance [5]. The mechanical strength of any welded product depends on its microstructural evolution, and therefore, several studies have already been performed to investigate the dissimilar welding of SS in the esteemed literature [6]. The microstructural investigation of the pulsed Nd: YAG laser welding of 17-4 PH steel reveals the formation of the lathy δ-Ferrite and interdendritic δ-Ferrite in the welded material [7]. The welding of the 17-4 PH SS can lead to the formation of solidification cracking. Preheating the material with a hybrid power source before actual welding significantly reduces solidification cracking [8]. The laser welding of the ASS 304 primarily leads to the formation of the small δ-Ferrite dendritic structures [9]. The presence and distribution of δ-Ferrite within the weld zone are of significant importance as it controls the joint strength and stability [10]. The formation and distribution of δ-Ferrite depends on various factors such as the material composition, cooling rate and solidification mode [11]. The dendritic size and spacing can be controlled by controlling the process parameters, which in

[1] DR. B. R. AMBEDKAR NATIONAL INSTITUTE OF TECHNOLOGY JALANDHAR, DEPARTMENT OF INDUSTRIAL AND PRODUCTION ENGINEERING, PUNJAB-144011, (INDIA)
[2] NATIONAL INSTITUTE OF TECHNOLOGY ROURKELA, DEPARTMENT OF INDUSTRIAL DESIGN ODISHA-769008, (INDIA)
[3] INDIAN INSTITUTE OF TECHNOLOGY GUWAHATI, DEPARTMENT OF MECHANICAL ENGINEERING, ASSAM – 781039, (INDIA)

* Corresponding author: bikash.kumar@iitb.ac.in

turn eventually controls the heat input [12]. Tushar et al., [13] investigated butt weld joints of super duplex stainless steel (UNS S32750) fabricated using different electrodes, i.e., ER2594 and ER2595 through arc welding (shielded metal arc welding, SMAW) process and observed austenite-ferrite solidification behaviour at fusion zone (FZ) and heat affected zone (HAZ). The microstructure was mainly composed of Widmanstatten austenite, inter- and intra-granular austenite. In another study, Tushar et al., [14] found varied heat affected zone width in the welded joints due to slight change in applied heat input from 0.75 → 0.81 J/mm. Additionally, Cr, Mo and Fe based precipitate was also obtained at molten zone, might be due to entrapment of different gases from the outer environment.

The numerical modelling of any manufacturing process provides a significant advantage in the in-process investigation of various thermo-mechanical responses and phase transformations. Initially, thermal and thermo-mechanical models were developed to predict the residual stresses and distortion in the plates [13]. Deng and Murakawa developed a numerical model to predict the residual welding stress by considering the phase transformation effects [14]. Further, the effect of phase transformation in the distortion and residual stresses for Ti-based alloy is also investigated [15,16]. Although various thermo-mechanical-metallurgical models are already disclosed for LBW in the literature, the numerical modelling of the dissimilar 17-4 PH SS and AISI 304 is not currently investigated.

Current investigation undertakes the assessment of Laser welded dissimilar AISI 304 to 17-4 PH SS. The thermo-microstructural anaylsis is performed for laser-welded dissimilar joints of 17-4 PH SS and AISI 304 and, its role in generation of residual stress is critically investigated via amalgamation of experiments and FE based numerical modeling approach. The key findings of our study revealed valuable insights into microstructural evolution of laser-welded 17-4 PH stainless steel during thermal exposure, shedding light on the mechanisms underlying phase transformations behavior. Additionally, we elucidated the impact of these microstructural changes on the mechanical properties, i.e., residual stress field of the dissimilar welded material. Our results provide important information for designing and optimizing laser-welding processes in the manufacturing of 17-4 PH stainless steel components, particularly in industries where thermal stability and mechanical integrity are critical factors.

2. Materials and experimental methods

Hot rolled sheets of 17-4 PH steel and SS 304 having a thickness of 0.7 mm were cut out into coupons of 70×60 mm^2 for producing efficient weld beads. The coupon surfaces were cleaned perfectly to remove the unwanted foreign impurities using acetone. The different material coupons are held firmly in butt configuration using a copper fixture in order to avoid the misalignment of the base materials and to achieve a superior weld solidification rate. The autogenous beads were prepared normal to the rolling direction of the sheets using CO_2 Laser source (2.5 kW continuous wave) over an extensive range of process parameters. The laser scanning rate, diameter of nozzle, and stand-off distance (SOD) are maintained constant at 700 mm/min, 0.25 mm and 15 mm, respectively, and laser beam offset of 1 mm distance towards SS-steel side was also taken into account for proper fusion of dissimilar plates, throughout the experimentation, whereas defocusing distance is varied between 0 and 1 mm. The Laser beam power has varied significantly between the ranges of 1200 W to 1800 W in order to achieve full penetration beads with minimum deformation. The optimised Laser power was found to be between 1500-1600 W through trial and error method where the produced beads were free from defects like partial penetration and excessive melting. The corresponding heat input per unit length is estimated to be between 128.5 J/mm to 160 J/mm for obtaining the successful welds using CO_2 Laser source. The successful beads are then processed for microstructural analysis through polishing and etching (in an acid solution of CH_3COOH: HCl: HNO_3) to reveal the microstructure of fusion zone and heat affected zone. The microstructural characterization was performed by using optical microscopy to analyse the formation and distribution of δ-ferrite in the weld zone.

3. Finite element modelling methodology

3.1. Heat transfer analysis

A 3-dimensional FE based thermal model is developed using commercial ABAQUS package for estimation of the time-temperature history of the weld pool. The following assumptions are considered in the numerical model for simplification. The weld top surface is considered as flat, by neglecting the effect of laser beam pressure on the flow of molten metal in the weld pool. The initial temperature (i.e., at T_0) of the parent materials is considered as 303K. The latent heat of fusion and solidification is considered in the numerical model and the molten metal evaporation is neglected in the fusion zone. The solution domain along with the boundary interaction for convective and radiative heat loss is shown in Fig. 1 for the considered dissimilar material combination. Optimal meshing arrangement is done in the solution domain to reduce the computational time. The DC3D8 type eight nodded brick elements are employed in the thermal model to incorporate diffusive heat transfer. Total of 191,921 number of nodes and 154,000 elements are generated for the solution domain for producing accurate and converged result. The Fourier's heat conduction based govering equations and associated thermal boundary condtions adopted for thermal analysis are extensively presented elsewhere [16].

3.2. Static stress analysis

The evaluated nodal time-temperature history from thermal analysis is applied as an input load for the estimation of thermo-

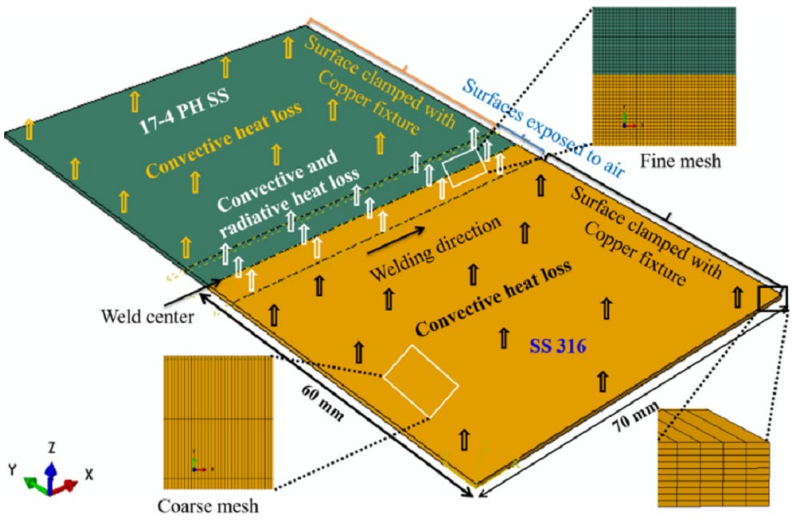

Fig. 1. Illustration of thermal boundary conditions incorporated during thermal modelling using ABAQUS commercial software

mechanical response of dissimilar welded joints of 17-4 PH steel and austenitic stainless steel. For this purpose, sequential coupled thermo-mechanical model is developed. Similar mesh specification as applied for thermal modelling, is considered for the structural analysis, however element changed to C3D8R for this analysis. Structural analysis is performed to assess the macroscopic residual stress behaviour of welded structures. The governing eauqations and corresponding mechanical boundary conditions are explained somewhere else [2].

The strain components which contribute to the genearation of residual stress is presented in the form of empirical relation in Eq. 1:

$$\epsilon_{ij}^{total} = \epsilon_{ij}^{elas} + \epsilon_{ij}^{plas} + \epsilon_{ij}^{therm} \quad (1)$$

where, ϵ_{ij}^{total} is the total strain responsible for the generation of residual stress. The ϵ_{ij}^{elas}, ϵ_{ij}^{plas} and ϵ_{ij}^{therm} represents strain associated with elastic, plastic and thermal component respectively. Fig. 2. represents the flow chart for the thermo-microstructural-mechanical study of dissimilar welded joints with the amalgamation of experimental and numerical approach. It also clarifies the steps and input which have been followed and taken, respectively for performing thermal as well as structural modelling.

4. Results and discussions

Fig. 3 demonstrates the interrelation between calculated heat input and corresponding welding performance for each process condition. Dissimilar metal joinining was obseved to be challenging compared to similar material welding. In dissimilar welding as the process progressed laser beam deflected from the fusion line towards base metal due to arch blow ten-

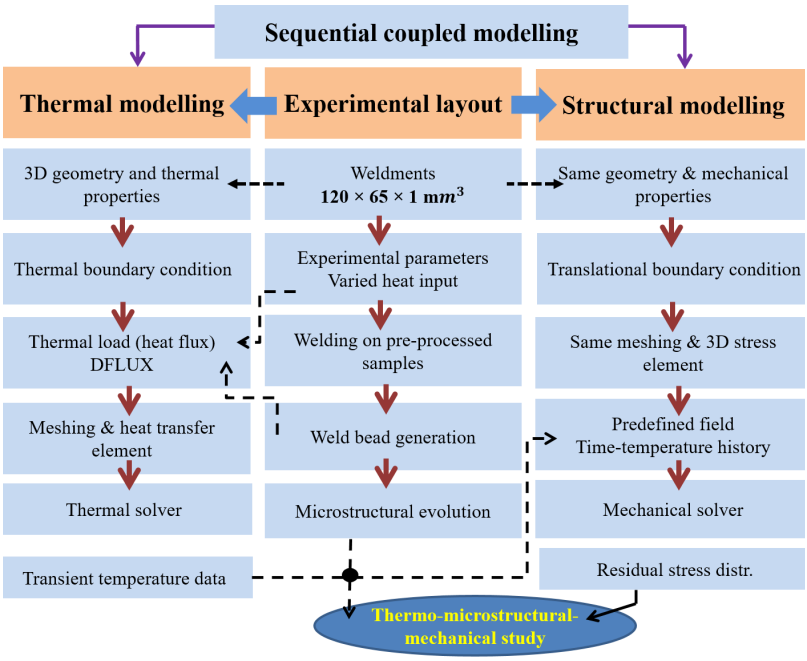

Fig. 2. Flow chart explaining the steps followed for thermal-microstructural-mechanical investigation

Specimens	Magnified bead	Process condition	Heat input	Remarks
(a) DS1		Power: 1200 Watt Welding speed: 700 mm/min Defocusing: 0 mm Offset: 1 mm	**102.8 J/mm**	**Insufficient fusion**
(b) DS2		Power: 1500 Watt Welding speed: 700 mm/min Defocusing: 0 mm Offset: 1 mm	**128.5 J/mm**	**Satisfactory depth of penetration**
(c) DS3		Power: 1600 Watt Welding speed: 600 mm/min Defocusing: 0 mm Offset: 1 mm	**160 J/mm**	**Full depth of penetration**
(d) DS4		Power: 1800 Watt Welding speed: 500 mm/min Defocusing: 1 mm Offset: 1 mm	**216 J/mm**	**Excessive melting**

Fig. 3 Bead evaluation of dissimilar 17-4 PH steel and austenitic stainless steel fabricated using varied heat input: (a) 102.8 J/mm; (b) 128.5 J/mm; (c) 160 J/mm; (d) 216 J/mm

dency. Hence, it is noted that the offset of laser beam by 1mm is taken into account for all the condition in order to get better sound quality weld for the dissimilar welding as suggested by several earlier published research. It is obvious that the depth of penetration is increased upon increasing heat input from 102 J/mm → 128 J/mm → 160 J/mm → 216 J/mm. At intial heat input of ~102 J/mm, insufficient fusion is observed owing to the inadequate energy density. Further, at the highest heat input of ~216 J/mm, broadended fusion zone, heat affected zone (HAZ) is observed due to excessive melting of metal. However, the weld joint fabricated at heat input of 160 J/mm is found to optimized one and exhibited sound quality weld.

Fig. 4 shows the heat flux distribution over the 3-Dimensional solution domain for dissimilar welded joints under vari-

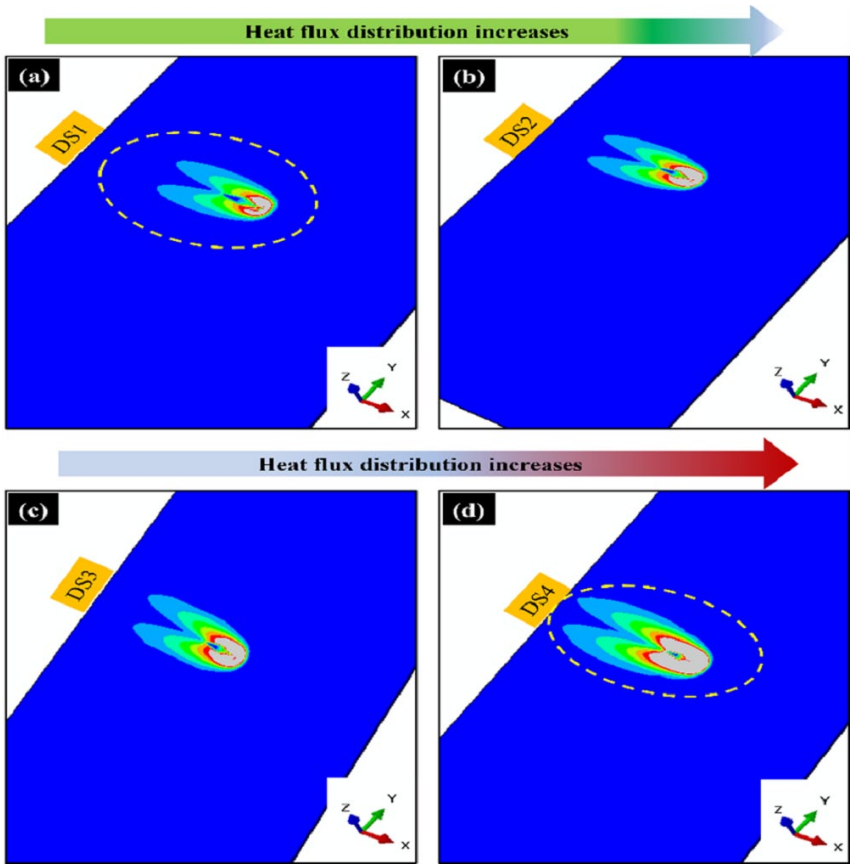

Fig. 4. Heat flux distribution onto the surface of three-dimensional solution domain corresponds to dissimilar weldments

ous process conditions. Rabbit-ear shaped flux distribution is obtained for all the fabricated structures. Since dissimilar plate welding are taken into account, therefore, two distinguished flux distribution is visibile in the given figure for each welding condition. Heat flux distribution is the deterministic factor that decides the overall temperature evolution in the molten pool and nearby region. Estimated heat flux is found to be of 10^7 W/ mm^2 for welded joints. It is observed that the heat flux distribution widens upon increasing heat input. Grey color contour represents the maxmum amount of heat flux which is in direct contact of laser beam that is highly localised or confined owing to fully converged laser beam.

Fig. 5 illustrates the three-dimensional contour of temperature evolved at weld zone and near by location during welding of dissimilar joint at various process conditions. The associated legend shows the maximum temperature of 1774 K, 2040 K, 2186 K and 2240 K exhibited by molten pool of weldments at heat input 102 J/mm, 128 J/mm, 160 J/mm and 216 J/mm, respectively. It should be noted that there is no significant difference in temperature distribution between PH-steel and austenitic steel has been observed, might be due to comparable thermo-physical properties for both the steel alloys. As the heat input progressed, the broadening of melt pool occured due to decrease in cooling rate. Due to high heat input, weld pool last for longer period of time which leads to the expansion of the molten pool. The temperature contour shows that each weld condition accomplished temperature sufficiently higher than that of melting temperature onto the surface, however temperature diffusion throughout the thickness is relatively less for lower heat input condition as confirmed by the Fig. 1.

Fig. 6 shows the nodal time-temperature history and corresponding location of measurement estimated through finite element based thermal modelling approach for dissimilar weld joint fabricated under optimized heat input condition i.e., 160 J/mm. Thermal characteristics is composed of heating and cooling cycle. Heating cycle is relatively steeper however, cooling cycle is gradual in nature, because heating rate is always greater than that of cooling rate. The unusual change of slope of temperature with time in cooling cycle is strong evidence of phase transformation behavior in the range of solidus and liquidus temperature. Time-temperature profile across the dissimilar weld joint at a distance of 0.5 mm, 1 mm, 1.5 mm and 2 mm is captured presented in figure (top side) at SS316 side and PH-steel side. Thermal cycle revealed that the temperature obtained at SS316 side is relatively higher than PH-steel side at each location. This is based on the fact that the melting temperature of SS316 is 10 degree less than PH-steel therefore more melting of material occurred from austenitic steel side which led to the enhancement of the temperature evolution. The investigated temperature decreased upon increasing the distance across the weld zone due to experiencing relatively less amount of heat input. Similar observation is also clarified in other study [16]. In the weld bead macrograph present at the bottom side, it is clearly depicted that the molten pool which possesses temperature beyond melting point, is shifted towards the SS-side by virtue of consideration of offset distance towards SS-side.

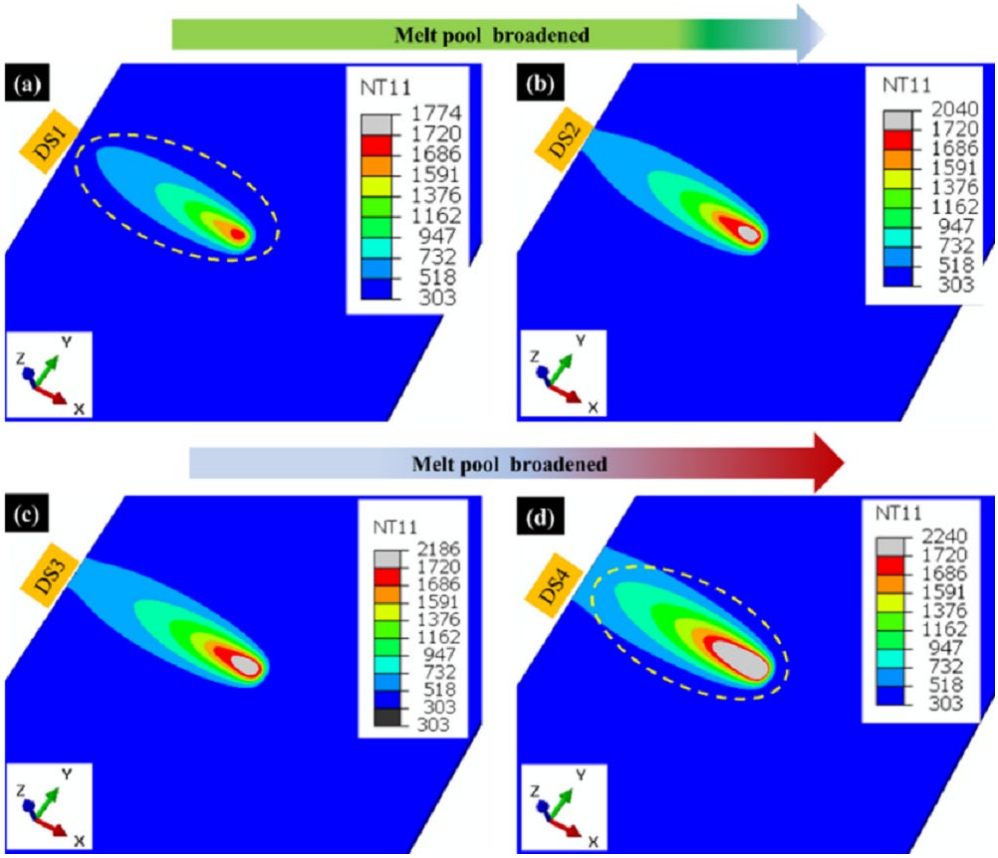

Fig. 5. Three-dimensional temperature distribution at the meltpool and far away location for different weld joints

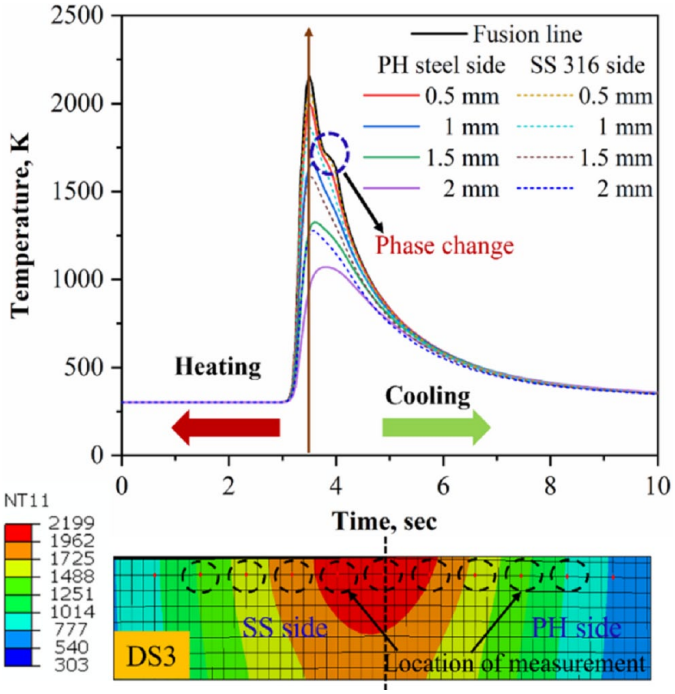

Fig. 6. Nodal time temperature history obtained across the weld line on SS316 side and PH-steel side, and representation of corresponding location of measurements over the cross-sectional temperature contour

Fig. 7 also clarifies that the temperature contour is somewhat bulged or shifted towards the stainless steel side due to offset distance that has been considered during the modelling. Crossectional profile of temperature distribution is not observed to be fully symmetric on SS316 and PH-steel side by virtue of difference in non-uniform temperature diffusion throughout the thickness.

Fig. 7 demonstrates the microstructural evolution during the welding of dissimilar joints. Full depth of penetration is clearly seen for the weld fabricated using heat input of 160 J/mm in the optical macroscopic image presented in Fig. 7a. Further, the partially melted region or transition zone is bounded by fusion zone and base metal area as shown in Fig. 7b. Unexpectedly, heat affected zone was not observed in welded sample on either side, i.e., SS316 side or 17-4 PH steel side. High cooling rate assisted laser based process and corresponding concentrated localised beam could be the reason due to which it has happened. Mixed mode of microstructure, i.e., ferrite-austenite structure is obtained in the fusion zone of welded joints fabricated using heat input of 128 J/mm and 160 J//mm as presented in Fig. 7c and d, respectively. Ferrite-austenite microstructure is exhibited due to incomplete transformation from δ-ferrite to γ-austenite. By comparing the Fig. 7c and d it is observed that the amount

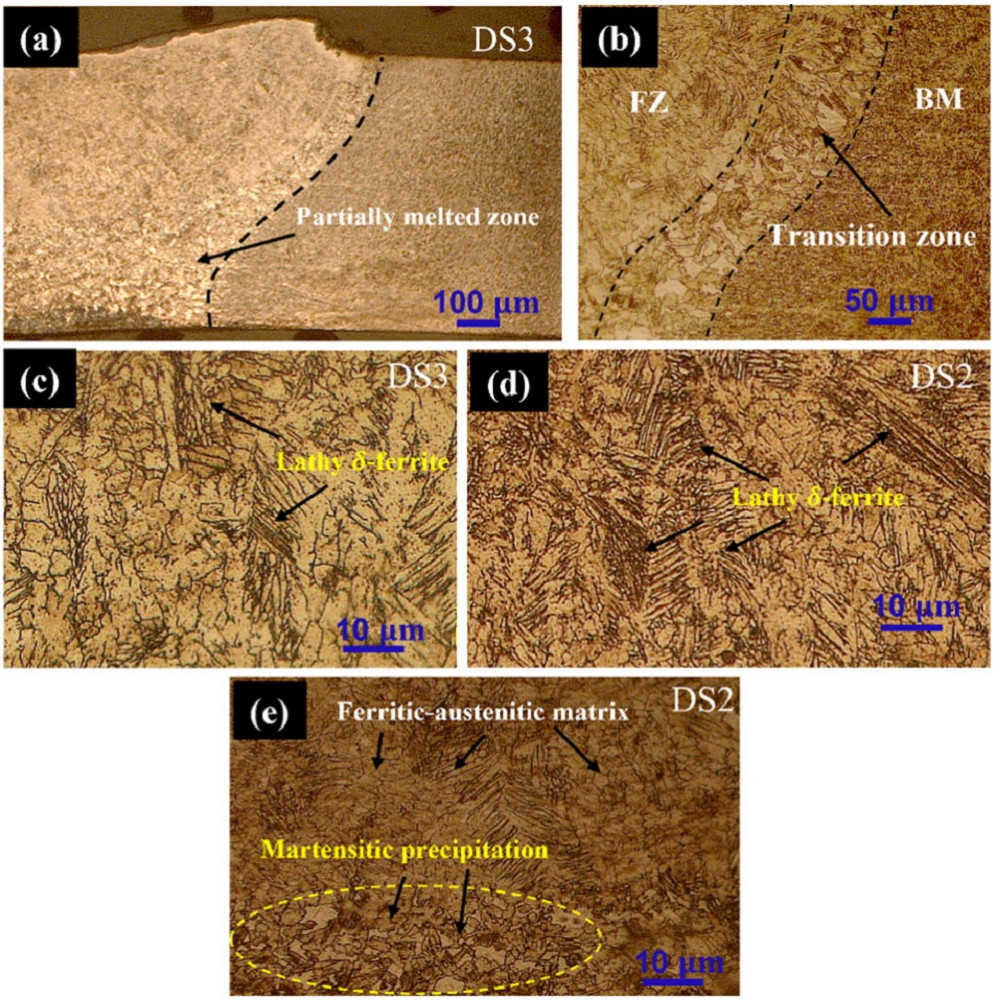

Fig. 7 (a) Macrostructural evolution at fusion zone, partially melted region and base metal; (b) magnified optical macrograph of partially melted region or transition zone; microstructural characteristics for weld metal: (c) DS3, (d) DS2; martensite precipitation at fusion zone of DS2 sample

of lathy δ-ferrite is relatively higher for DS2 (128 J/mm) rather than DS3 (160 J/mm). High heat input provides a platform for significant transformation from δ-ferrite to γ-austenite. Hence, DS2 sample fabricated using lower amount of heat input exhibited higher amount of δ-ferrite phase fraction. Further, Fig. 7e holds a austenitic-ferritic microstructure with matensitic precipitates distributed in the austenitic matrix. High cooling rate associated with lower heat input favours diffusionless martensitic transformation, which can exhibits better weldability, improved strength and excellent corrsion resistance [15].

Fig. 8 represents the longitudinal residual stress distribution for dissimilar welded joints fabricated using 102 J/mm and 160 J/mm. Relatively high residual stress of ~330 MPa is experienced on the austenitic stainless steel side, whereas 295 MPa is obtained on 17-4 PH steel side. Martensite precipitation on PH steel side put the fusion zone in compression state owing to volumetric expansion which minimised the overall tensile residual stress of the structure on PH steel side. The figure also clarifies that the observed residual stress is found to be less for low heat input condtion, i.e., 102 J/mm sample. Less heat input can reduce the chances of experiencing high temperature gradient which is the most prominent cause of residual stress, hence it is found to be lower for low heat input condition. In order to maintain structural equilibrium tensile stress is compensated with consequtive compressive stress on either side of the structure. The thermal expansion coefficient of Ni (austentic stabilizer) is ~1.5 times higher than the Cr (ferritic stabilizer) due to which austenitic region exhibits micro-tensile stress whereas, Cr-region accomplishes compressive stress. Sample welded using high input acquired higher austentic fraction than ferrite, therefore the chances of experiencing tensile stress is more for high heat input condition, this might be the another explanation for achieving more tensile stress for 160 J/mm rather than 102 J/mm. similar conclusion hase been drawn by Kumar et al., in their study [2].

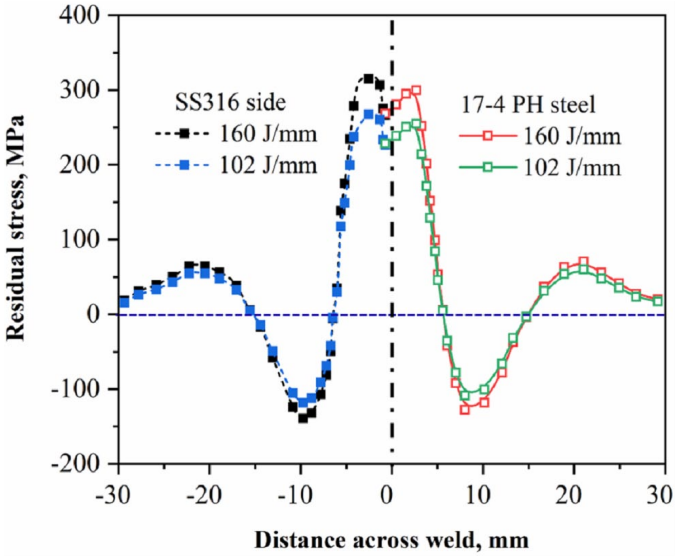

Fig. 8. Longitudinal residual stress distribution over the dissimilar welded joints for the heat input of 160 and 102 J/mm

5. Conclusions

Dissimilar joints of 17-4 PH steel and austenitic stainless steel (SS316) is performed using different heat input conditions. Thermo-microstructural-mechanical behaviour of welded joints are extensively studied using experimentations and finite element based numerical modelling approach. The following conclusions have been drawn thorugh the above study**:**

- Heat input of 160 J/mm is observed to be optimized process condition (as sound weld with full depth of penetration is obtained) for the fabrication of dissimilar joint of 17-4 PH steel and SS316 steel.
- Broadening of molten pool is obtain upon increasing heat input owing to higher temperature evolution and associated lower cooling rate characteritics.
- The maximum temperature attained at SS316 side is somewhat higher than 17-4 PH steel by virtue of differenrce in thermo-physical properties.
- Precipitation of martensite is clearly seen in the austenitic-ferritic matrix at fusion zone for lower heat input condition due to material mixing of precipitate hardened steel with austentic stainless steel in the course of welding.
- Higher fraction of ferrite and precipitation of martensite put the weld zone in compressive stress state that minimized the overall tensile stress behaviour of welded structure for relatively low heat input condition, i.e., 102 J/mm.

Acknowledgement

I would like to thanks the department of mechanical engineering, Indian Institute of Technology Guwahati for providing experimental facility to perform the required expriments.

REFERENCES

[1] S. Sirohi, S.M. Pandey, V. Tiwari, D. Bhatt, D. Fydrych, C. Pandey, Impact of laser beam welding on mechanical behaviour of 2.25Cr–1Mo (P22) steel. Int. J. Press. Vessel. Pip. **201**, October 2022, 104867 (2023).
DOI: https://doi.org/10.1016/j.ijpvp.2022.104867

[2] B. Kumar, S. Bag, S. Mahadevan, C.P. Paul, C.R. Das, K.S. Bindra, On the interaction of microstructural morphology with residual stress in fiber laser welding of austenitic stainless steel. CIRP J. Manuf. Sci. Technol. **33**, 158-175 (2021).
DOI: https://doi.org/10.1016/j.cirpj.2021.03.009

[3] A.K. Sahu, S. Bag, Influence of heat input on intermetallic formation in dissimilar autogenous laser welding between Inconel 718 and AISI 316L steel. Proc. Inst. Mech. Eng. Part B J. Eng. Manuf. September (2022).
DOI: https://doi.org/10.1177/09544054221129463

[4] X. Lin, Y. Cao, X. Wu, H. Yang, J. Chen, W. Huang, Microstructure and mechanical properties of laser forming repaired 17-4PH stainless steel. Mater. Sci. Eng. A **553**, 80-88 (2012). DOI: https://doi.org/10.1016/j.msea.2012.05.095

[5] F.F. Curiel, R. García, V.H. López, J. González-Sánchez, Effect of magnetic field applied during gas metal arc welding on the resistance to localised corrosion of the heat affected zone in AISI 304 stainless steel. Corros. Sci. **53**, 7, 2393-2399 (2011). DOI: https://doi.org/10.1016/j.corsci.2011.03.022

[6] E.M. Anawa. A.G. Olabi, Optimization of tensile strength of ferritic/austenitic laser-welded components. Opt. Lasers Eng. **46**, 8, 571-577 (2008). DOI: https://doi.org/10.1016/j.optlaseng.2008.04.014

[7] M. Bahrami Balajaddeh, H. Naffakh-Moosavy, Pulsed Nd:YAG laser welding of 17-4 PH stainless steel: Microstructure, mechanical properties, and weldability investigation. Opt. Laser Technol. **119**, June (2019). DOI: https://doi.org/10.1016/j.optlastec.2019.105651

[8] W. Liu et al., Hybrid Laser-arc Welding of 17-4 PH Martensitic Stainless Steel, Lasers Manuf. Mater. Process. **2**, 2, 74-90 (2015). DOI: https://doi.org/10.1007/s40516-015-0007-2

[9] J. Yan, M. Gao, X. Zeng, Study on microstructure and mechanical properties of 304 stainless steel joints by TIG, laser and laser-TIG hybrid welding. Opt. Lasers Eng. **48**, 4, 512-517 (2010). DOI: https://doi.org/10.1016/j.optlaseng.2009.08.009

[10] R. Unnikrishnan et al., Effect of heat input on the microstructure, residual stresses and corrosion resistance of 304l austenitic stainless steel weldments. Mater. Charact. **93**, 10-23 (2014). DOI: https://doi.org/10.1016/j.matchar.2014.03.013

[11] P.S. Korinko, S.H. Malene, Considerations for the weldability of types 304L and 316L stainless steel. J. Fail. Anal. Prev. **1**, 4, 61-68 (2001). DOI: https://doi.org/10.1007/BF02715336

[12] S. Kumar, A.S. Shahi, Effect of heat input on the microstructure and mechanical properties of gas tungsten arc welded AISI 304 stainless steel joints. Mater. Des. **32**, 6, 3617-3623 (2011). DOI: https://doi.org/10.1016/j.matdes.2011.02.017

[13] T.R. Dandekar, A. Gupta, R.K. Khatirkar, R. Kumar, A.D. Gaikwad, Evolution of microstructure and texture in UNS S32750 super duplex stainless steel weldments. Trans. of the Indian Inst. of Metals **74**, 9, 2267-2283 (2021). DOI: https://doi.org/10.1007/s12666-021-02274-x

[14] T.R. Dandekar, A. Gupta, A. Kumar, R.K. Khatirkar, B. Vadavadagi, Shielded metal arc welding of UNS S32750 steel: microstructure, mechanical properties and corrosion behaviour. Materials Research Express **5**, 10, 106506 (2018). DOI: https://doi.org/10.1088/2053-1591/aad99a

[15] G.A. Moraitis, G.N. Labeas, Prediction of residual stresses and distortions due to laser beam welding of butt joints in pressure vessels. Int. J. Press. Vessel. Pip. **86**, 2-3, 133-142 (2009). DOI: https://doi.org/10.1016/j.ijpvp.2008.11.004

[16] D. Deng, H. Murakawa, Influence of transformation induced plasticity on simulated results of welding residual stress in low temperature transformation steel. Comput. Mater. Sci. **78**, 55-62 (2013). DOI: https://doi.org/10.1016/j.commatsci.2013.05.023

[17] B. Kumar, S. Bag, Phase transformation effect in distortion and residual stress of thin-sheet laser welded Ti-alloy. Opt. Lasers Eng. **122**, 209-224 (2019). DOI: https://doi.org/10.1016/j.optlaseng.2019.06.008.

[18] B. Kumar, S. Bag, C.P. Paul, C.R. Das, R. Ravikumar, K.S. Bindra, Influence of the mode of laser welding parameters on microstructural morphology in thin sheet Ti6Al4V alloy. Opt. Laser Technol. **131**, 106456, July (2020).